Electronic Supplementary Material (ESI) for Nanoscale.

Supporting Information for Ultrafast Hot Electron-Hole Plasma Photoluminescence in Two-Dimensional Semiconductors

Frederico B. Sousa, Raül Perea-Causin, Sean Hartman, Lucas Lafetá, Bárbara Rosa, Samuel Brem, Chirag Palekar, Stephan Reitzenstein, Achim Hartschuh, Ermin Malic, and Leandro M. Malard.

This Supporting Information includes:

Section S1. Raman and Photoluminescence Spectroscopy Measurements

In order to further characterize the WSe_2 samples used in this work we performed Raman and photoluminescence (PL) measurements. Figures S1a-d show the Raman spectra for the monolayer, bilayer, trilayer and bulk WSe2, respectively. The spectra display the characteristic E^1_{2g} and A_{1g} Raman modes of the WSe2 samples around 250 cm^{-1} besides their 2LA peak at $\sim$ 257 cm^{-1}. Nonetheless, due to the degeneration of these two first order peaks these measurements are not convenient to determine the number of layers of each sample. On the other hand, PL measurements have been widely used to ascertain the thickness of WSe2 samples as previously reported by several authors.[1–3] Figure S2a-d respectively presents the PL spectra of the same monolayer, bilayer, trilayer and bulk WSe2. It can be noticed that the monolayer shows a strong emission from its trion (X^-) and exciton (X) bound states. In the multilayers spectra, beyond the direct optical transition (DT) we can also note an emission from their indirect transition (IT). Furthermore, there is a redshift of both direct and indirect peaks while increasing the sample thickness. All the peak positions together with the relative PL intensity between the samples are in agreement with our sample thickness assignment by comparing to the well established literature for that. The Raman and PL peak positions for all the samples are shown in Table 1.

Table 1: Peak Positions

	1L-WSe_2	2L-WSe_2	3L-WSe_2	Bulk-WSe_2
E^1_{2g}/A_{1g}	248.6 cm^{-1}	249.8 cm^{-1}	250.8 cm^{-1}	251.0 cm^{-1}
2LA	257.1 cm^{-1}	257.6 cm^{-1}	258.1 cm^{-1}	258.3 cm^{-1}
PL DT (or X)	1.67 eV	1.63 eV	1.59 eV	1.53 eV
PL IT (or X^-)	1.64 eV	1.55 eV	1.46 eV	1.37 eV

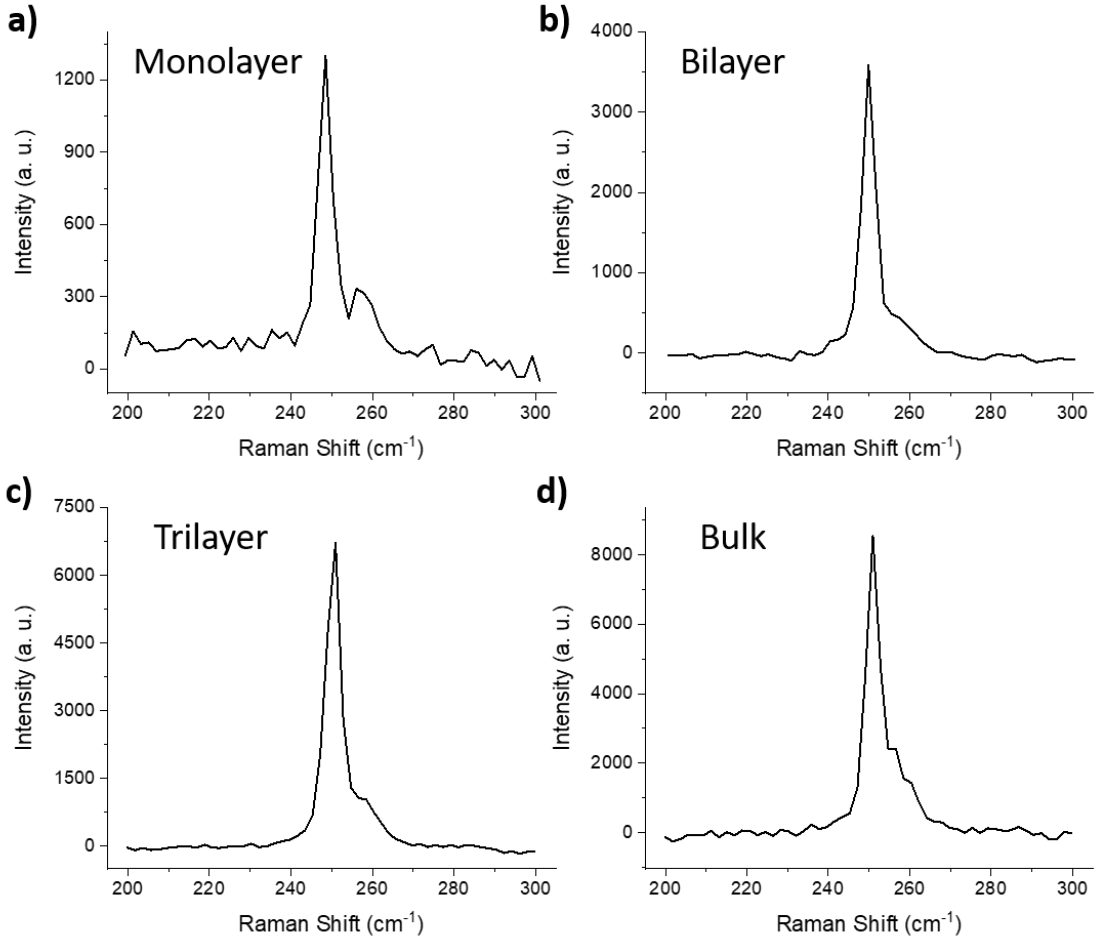

Figure S1: Raman spectroscopy measurements of WSe_2 samples. **a-d** Raman spectrafor the monolayer (**a**), bilayer (**b**), trilayer (**c**), and bulk (**d**) WSe_2 showing their degenerated E^1_{2g} and A_{1g} and 2LA peaks. The measurements were carried out with a 561 nm excitation and an incident power of 0.6 mW.

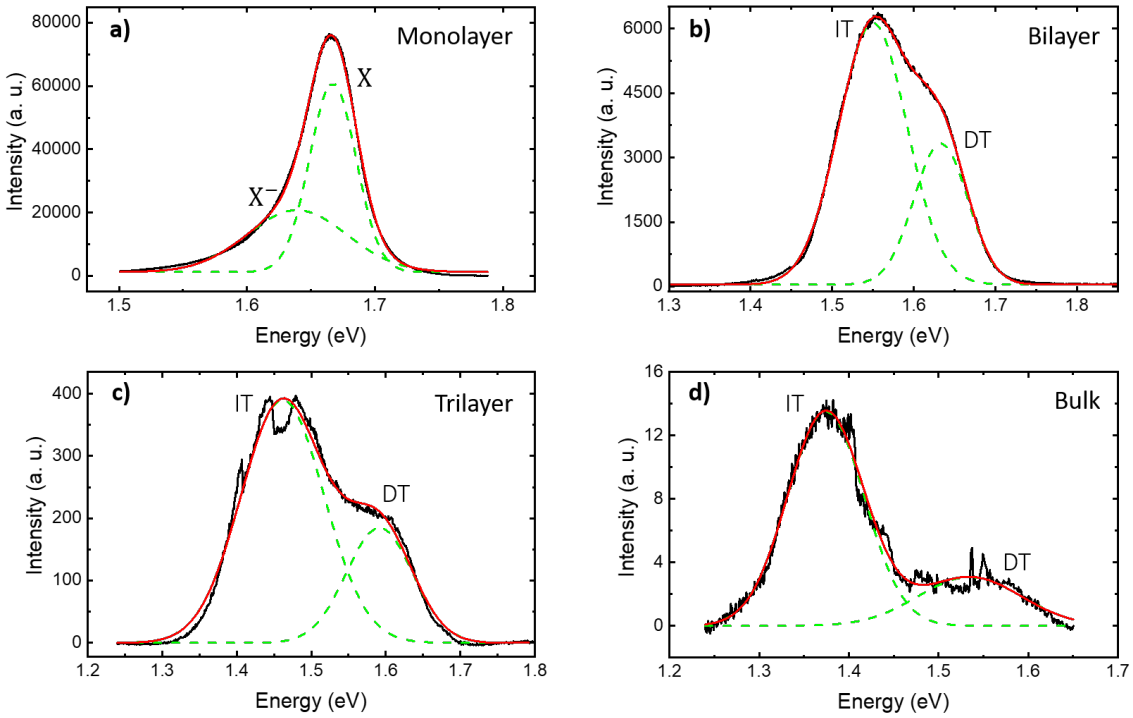

Figure S2: PL spectroscopy measurements of WSe_2 samples. **a-d** PL spectra for the monolayer (**a**), bilayer (**b**), trilayer (**c**), and bulk (**d**) WSe_2. It can be observed the reported shift in the peak positions and also the intensity decrease by increasing the number of layers. The spectra were fitted by two Gaussian peaks that are accounted to trion (X^-) and exciton (X) for the monolayer and indirect (IT) and direct (DT) transitions for the multilayers. The measurements were carried out with a 561 nm excitation and an incident power of 0.6 mW.

Section S2. Substrate Peak Removal

Figure S3 shows the light emission spectra of the quartz substrate under a pulsed excitation with an energy of 1.58 eV for the same incident powers used to probe the WSe_2 samples (Figures 1 and 2 of the manuscript). We can observe a significant signal around 1.4 eV. This substrate signal has also appeared in the monolayer, bilayer, trilayer and bulk WSe_2 PL spectra as can be seen in Figure S4. In order to extract this substrate contribution to focus only in the sample emission, for each pump power we subtracted the quartz spectra from the samples spectra. The oscillations observed in the PL spectra of Figures 1 and 2 of the manuscript around the substrate peak are presumably due to changes in the quartz signal with and without the sample on the top.

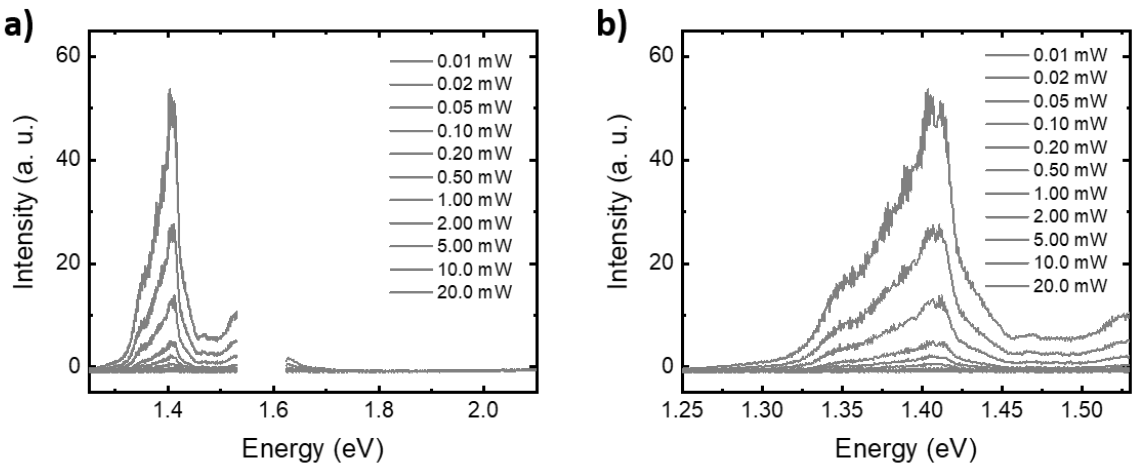

Figure S3: Light emission from the quartz substrate under a pulsed excitation for distinct incident powers. In (a) it is shown the whole spectra while in (b) it is highlighted the substrate peak around 1.4 eV.

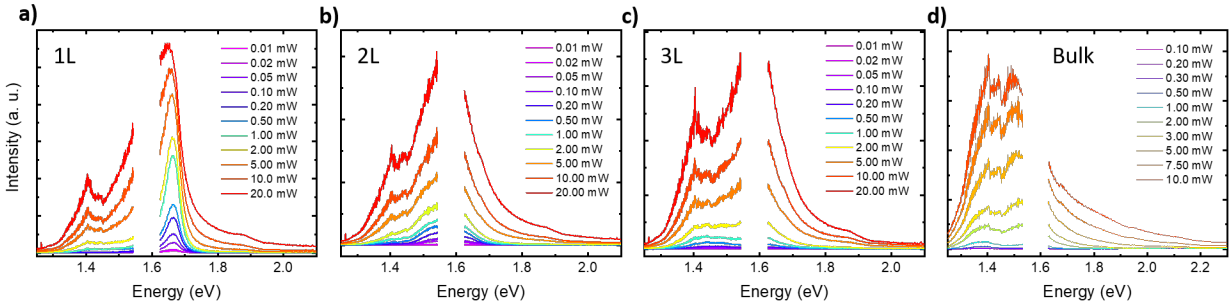

Figure S4: Raw PL spectra of a monolayer (**a**), bilayer (**b**), trilayer (**c**) and bulk (**d**) WSe_2. The substrate peak around 1.4 eV can be noted for all spectra.

Section S3. Power Dependence of the PL Intensity under CW Excitation

As commented in the manuscript, the PL measurements of the monolayer WSe_2 under CW excitation shown in Figures 1a,b display an approximately linear dependence with the incident power as shown in Figure S5.

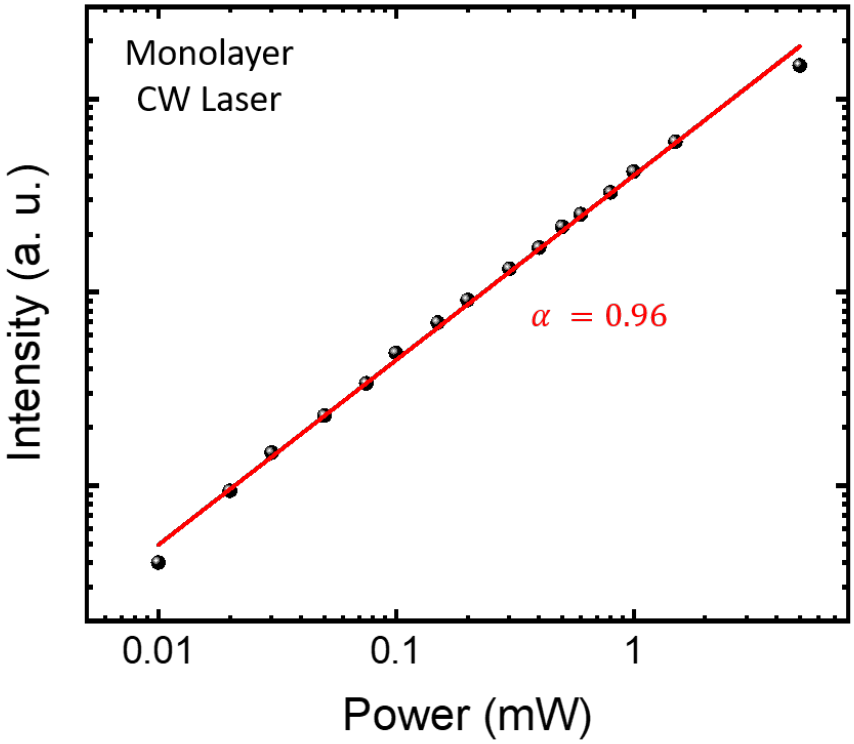

Figure S5: Power dependence of the photoluminescence (PL) intensity of a monolayer WSe_2 under CW excitation. The 0.96 coefficient shows the linear dependence with the incident power. The axes are in a logarithm scale.

Section S4. Excitation Energy Dependence of the EHP PL

To check if the pulsed excitation PL was generated by an one or two photon absorption process we performed excitation energy dependent PL measurements as presented in Figure S6. All measurements were carried out with the same pump power of 2 mW. We observe that decreasing the excitation energy the PL signal is also decreased, vanishing around an excitation at 1.5 eV. It is an evidence of an one photon absorption, since this PL intensity quenching would not be expected for a two photon absorption as discussed in the manuscript. On the other hand, a second-harmonic generation (SHG) emission is also noted even for the low excitation energies, reinforcing the absence of a two photon absorption EHP PL for these energies.

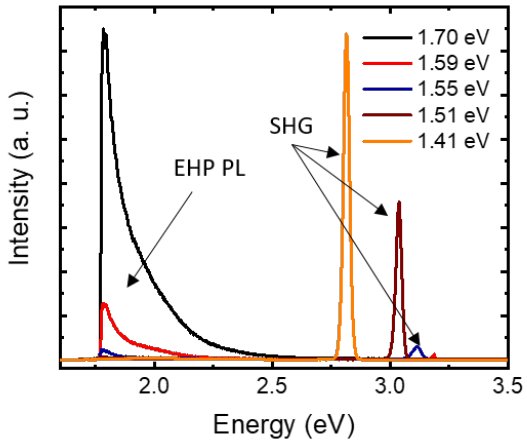

Figure S6: Excitation energy dependence of the EHP PL intensity of a monolayer WSe_2 under pulsed excitation.

Section S5. Carrier Densities Calculation

The charge carrier density n_0 (cm^{-2}) generated under a pulsed excitation was calculated by:[4]

$$n_0 = \frac{P \cdot \sigma}{A \cdot f_{rep} \cdot E}; \quad (1)$$

in which P is the incident laser power (W), σ is the absorptance taken from Yiley *et al.*,[5] A is the area (cm^2) of the spot of the laser at the sample, f_{rep} is the laser pulse repetition rate (s^{-1}), and E is the incident photon energy (J). It is worth to mention that the pump fluence used in the manuscript is the reason between P with the product of A with f_{rep}, being A in m^2 in this case. Therefore, we took the Mott critical pump fluence value from the PL broadening in Figure 1f of the manuscript and calculated its corresponding carrier density.

We have to point that this calculated Mott critical carrier density is an approximation due to the use of a constant σ. As shown in Section 6 of this Supporting Information, we observed that the absorbed power does not have a linear dependence with the total incident power. Furthermore, the excitation-induced dephasing can also play a minor role in the PL broadening,[6] thus affecting the estimation of the critical pump fluence value in Figure 1f of the manuscript. Therefore, this approximation is only reliable to provide the order of magnitude of the critical density for the Mott transition.

Section S6. Sample Preservation after a High Excitation Density

We performed SHG imaging, Raman spectroscopy and low-power PL spectroscopy in a monolayer WSe_2 before and after the EHP PL measurements to probe the sample preservation after the high excitation fluences. The SHG images S7 show the preservation of the signal uniformity even after a laser irradiation of 10 mW (120 J/m2). However, for pump powers above this value the sample starts to be burned as can be noted in the most left SHG image. Likewise, the Raman and PL features were preserved until an incident power of 20 mW, when they presented a quenching in the intensity and the PL also displayed a significant shift. Thus, we observed a sample preservation even after a high-density excitation of one order of magnitude above the Mott transition density. These high pump powers are possible due to the sub-band gap excitation energy, which lead to a lower absorption and no damage in the sample.

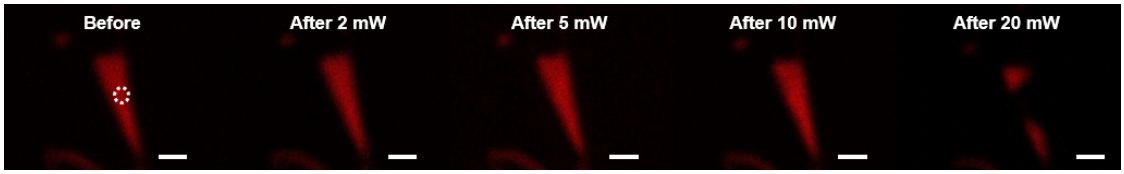

Figure S7: SHG imaging in a monolayer WSe_2 before and after the EHP PL measurements with pump powers of 2, 5, 10 and 20 mW. The dashed circle in the first image shows the position where the sample was exposed with the different high power laser irradiation. Scale bar: 2μm

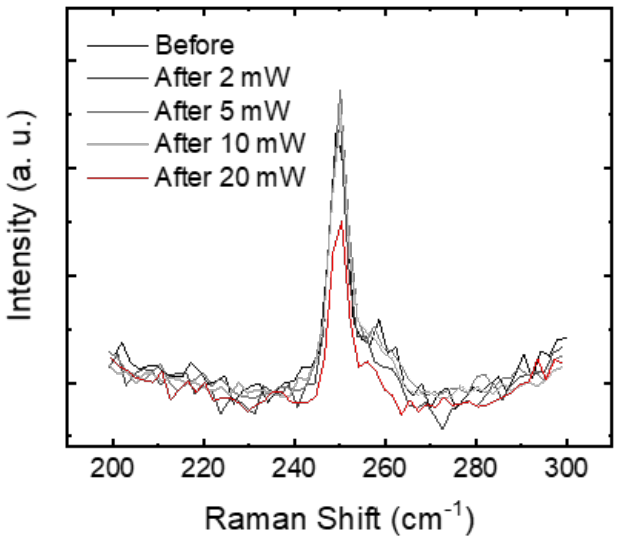

Figure S8: Raman measurements in a monolayer WSe_2 before and after the EHP PL measurements with pump powers of 2, 5, 10 and 20 mW.

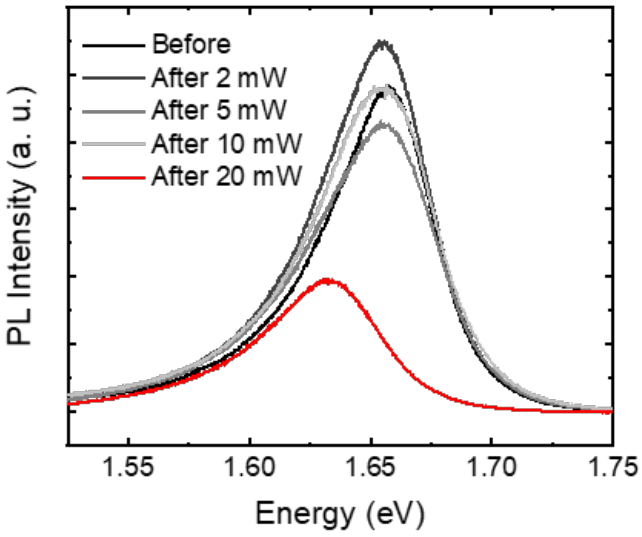

Figure S9: Low-power PL measurements in a monolayer WSe_2 before and after the EHP PL measurements with pump powers of 2, 5, 10 and 20 mW.

Section S7. Pump Power Dependence of the PL FWHM in Multilayer WSe_2

Figures S10a-c show the pump power dependence of the pulsed excitation PL full width at half maximum (FWHM) of the multilayer WSe_2 samples shown in Figure 2 of the manuscript. To verify the asymmetric broadening the peak maximum value was considered as the indirect transition peak maximum for all incident power. We can note that for all samples there is a critical pump power in which the FWHM starts to increase revealing the exciton Mott transition to an EHP phase.

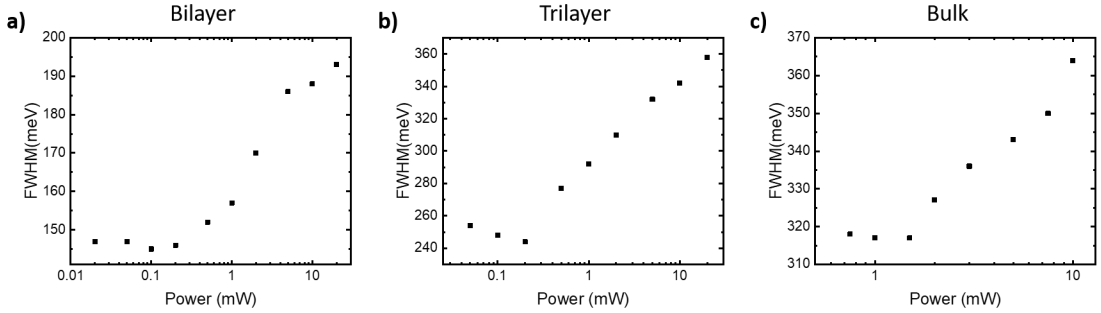

Figure S10: **a-c** Power dependence of the PL FWHM in a bilayer (**a**), trilayer (**b**) and bulk (**c**) WSe_2 samples. For all samples there is a critical pump power value in which the FWHM starts to increase revealing the exciton Mott transition to an EHP phase.

Section S8. Sample Thickness Dependence of the PL Intensity

Figures S11a-d gather the PL spectra under pulsed excitation of the monolayer, bilayer, trilayer, and bulk WSe_2 presented in Figures 1 and 2 of the manuscript for incident powers of 0.01, 0.1, 1.0, and 10 mW, respectively. For the excitonic regime, the monolayer signal is considerably stronger than the multilayer samples (for an incident power of 0.01 mW the bulk sample did not even show any PL signal). Nonetheless, in the EHP regime the multilayer samples PL becomes comparable (or even greater for the bulk sample) with respect to the monolayer emission. It happens due to the presumable indirect to direct band gap transition in the multilayers WSe_2 with the carrier density enhancement.

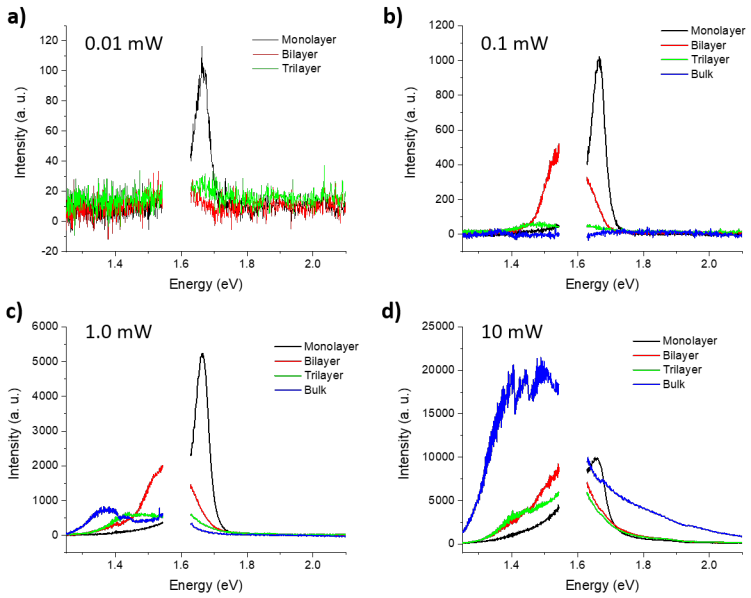

Figure S11: Sample thickness dependence of the PL intensity under a pulsed excitation. **a-d** PL spectra of a monolayer, bilayer, trilayer and bulk WSe_2 for an incident power of 0.01 mW (**a**), 0.1 mW (**b**), 1.0 mW (**c**), and 10 mW (**d**). It can be noted that while the monolayer present a much greater PL intensity with respect to the multilayer samples for a low carrier density regime, the intensities of all samples become similar when they are excited to the EHP phase.

Section S9. The Nonlinearity of the EHP Emission

As discussed in the manuscript, the EHP phase generated by the pulsed excitation at high pump fluences present a nonlinear light emission. Figure S12 shows the EHP PL pump fluence dependence of a monolayer WSe_2 for distinct excitation energies. The graphs in the left side display the spectra taken with distinct incident powers in the low electronic occupation range above the material band gap for excitation energies of 1.70 (Figure S12a), 1.59 (Figure S12c), 1.55 (Figure S12e), and 1.51 eV (Figure S12g). The graphs in the right side present the respective pump fluence PL dependence, showing that the nonlinearity increases by pumping the sample with a lower excitation energy. It is worth to comment that although the the PL behavior for the 1.70 eV excitation energy seems to be linear (Figure S12b), what is probably happening is that the absorbed fluence (that is what really matters for this relation) is proportionately decreasing when we increase the total incident fluence, *i.e.*, the greater the pulsed incident fluence the lower the proportional absorption. Therefore, the coefficients that we take from the fits in the right side graphs of Figure S12 are probably smaller than the real nonlinear values. This is confirmed by the fluence dependent second harmonic generation (SHG) measurements shown in Figure S13. While the expected SHG power law exponent is 2, we observe a smaller value due to that explained above.

Figure S14 shows similar measurements for the bulk WSe_2 for excitation energies of 1.70 (Figures S14a,b) and 1.55 eV (Figure S14c,d). It can also be observed a nonlinear dependence of the EHP PL intensity with the pump fluence. Moreover, it can be noticed that the bulk sample present a stronger nonlinearity in comparison with the monolayer. As shown in the manuscript, this feature is also present in the two-pulse correlation measurements of these two samples.

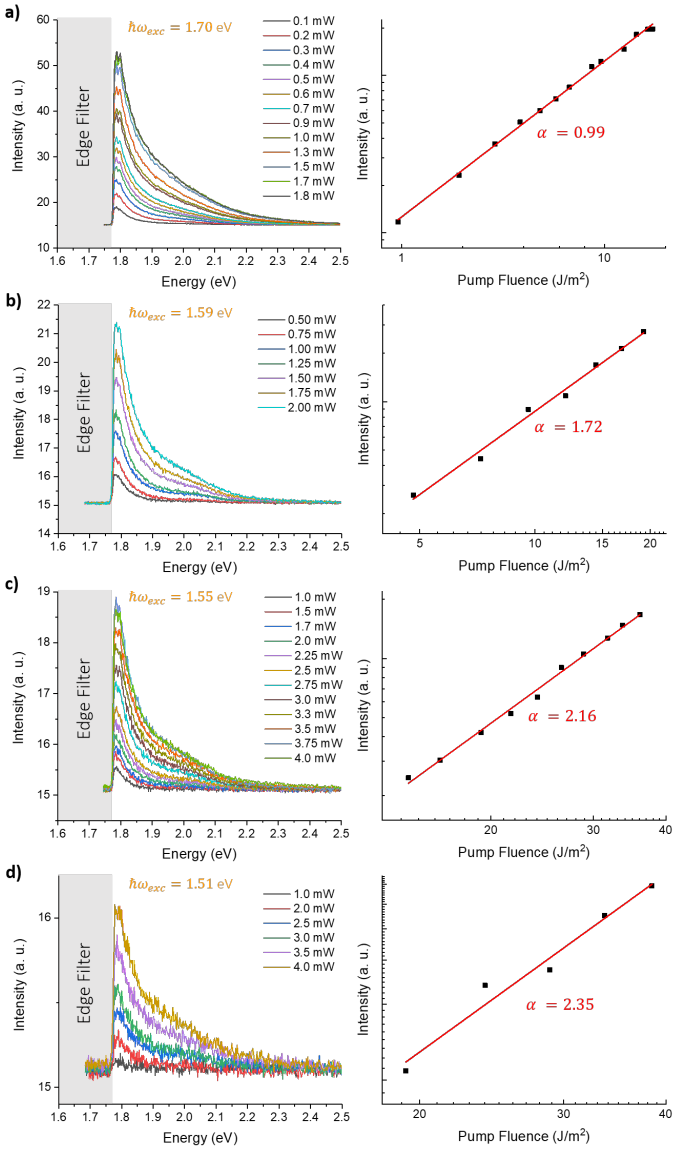

Figure S12: Nonlinear pump fluence dependence of the EHP PL for distinct excitation energies of a monolayer WSe_2. **a-d** PL spectra above the band gap (left side graphs) of a monolayer WSe_2 and their pump fluence dependence (right side graphs) for energy excitations of 1.70 eV (**a**), 1.59 eV (**b**), 1.55 eV (**c**), and 1.51 eV (**d**). It can be seen that the lower the excitation energy, the greater the nonlinearity of the effect. The axes of the right side graphs are displayed in a logarithm scale.

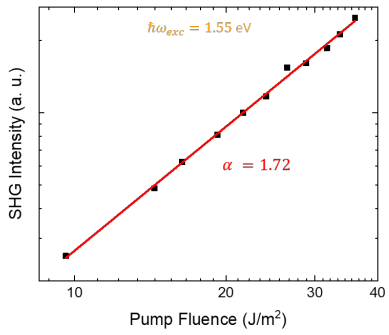

Figure S13: Nonlinear pump fluence dependence of the SHG for an excitation energy of 1.55 eV in a monolayer WSe_2. Unlike the expected, the power law exponent is less than 2 (1.72). This is explained by the decreasing in the proportional absorbed power by increasing the total incident power. The axes are displayed in a logarithm scale.

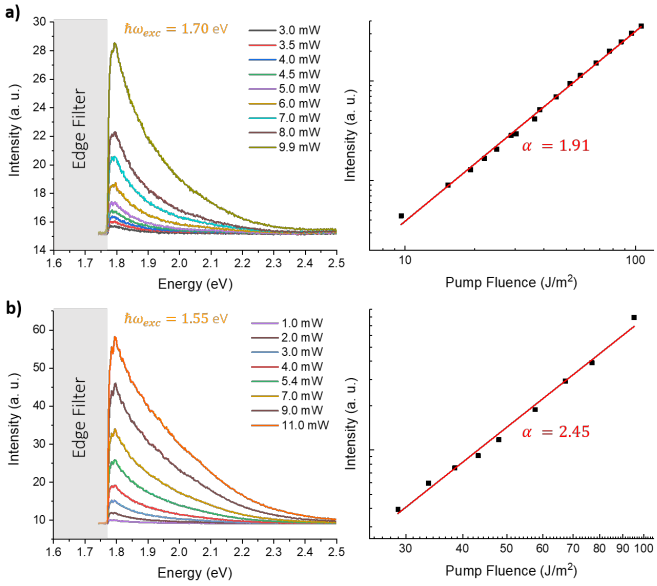

Figure S14: Nonlinear pump fluence dependence of the EHP PL for distinct excitation energies of a bulk WSe_2. **a-b** PL spectra above the band gap (left side graphs) of a bulk WSe_2 and their pump fluence dependence (right side graphs) for energy excitations of 1.70 eV (**a**) and 1.55 eV (**b**). It can be seen that the lower the excitation energy, the greater the nonlinearity of the effect. Furthermore, it can also be noted that the EHP PL in the bulk sample is more nonlinear than in the monolayer sample. The axes of the right side graphs are displayed in a logarithm scale.

Section S10. Bilayer and Trilayer WSe_2 two-pulse excitation correlation measurements

The two-pulse excitation correlation measurements were also perfomed for the bilayer and trilayer WSe_2 samples as shown in Figure S15. While both samples displayed the same ultrafast time response of less than 100 fs accounted to the electron-phonon thermalization, the bilayer presented a slower decay time of ~ 3 ps and the trilayer ~ 4 ps due to the electron-phonon thermal equilibrium with the lattice bath.

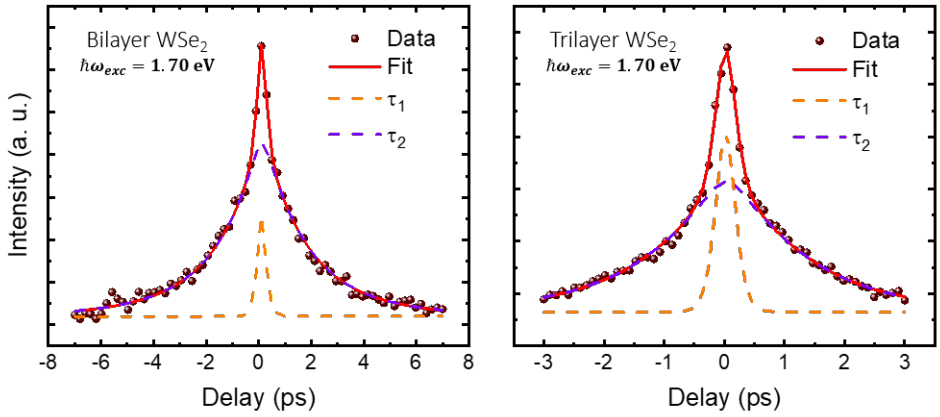

Figure S15: Two-pulse excitation correlation measurement in a bilayer and trilayer WSe_2. The scatter data show the intensity profiles of the PL signal of the WSe_2 samples with respect to the temporal delay between the incident laser pulses. We collected only the energies at 1.97 eV (above the band gap) by using a combination of shortpass and bandpass filters. The temporal fit is shown in red, while the separated contributions of both time responses are displayed in the orange and purple dashed lines. It is observed a fast time scale of less than 100 fs and a slower one of ~ 3 and ~ 4 ps for the bilayer and trilayer, respectively.

Section S11. Monolayer $MoSe_2$ Measurements

Here we show that the monolayer $MoSe_2$ also behaves similarly to the WSe_2 samples under pulsed excitations at high pump fluences. Figures S16a,b show the EHP PL spectra for distinct incident powers and for pulsed excitation energies of 1.53 and 1.49 eV, respectively. These spectra were taken in the low electronic occupation range above the material band gap. In Figures S16c,d it can be observed that the light emission under a pulsed excitation is indeed broadened with respect to the CW excitation, revealingt the monolayer $MoSe_2$ exciton Mott transition into an EHP phase as well as shown by the WSe_2 samples. Moreover, Figures S16e,f also show the nonlinearity of the effect and how it is increased by decreasing the excitation energy.

We have also probed the dynamics of the EHP PL in the monolayer $MoSe_2$ by performing a two-pulse excitation correlation measurement on it. Figure S17 shows that the correlation time scales of the monolayer $MoSe_2$ are very similar to the WSe_2 monolayer ones. There is an ultrafast time response of less than 100 fs accounted to the electron-phonon thermalization and a slower one of ~ 4 ps due to the electron-phonon thermal equilibrium with the lattice bath.

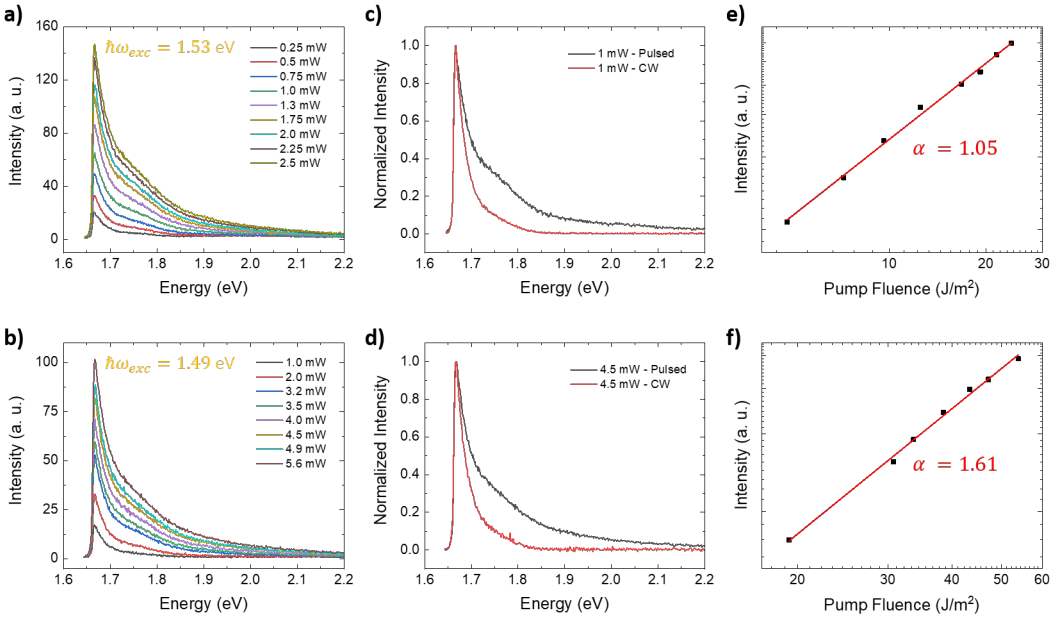

Figure S16: Monolayer $MoSe_2$ PL in the EHP regime. **a-b** PL spectra above the band gap of a monolayer $MoSe_2$ for distinct incident powers for pulsed excitation energies of 1.53 eV (**a**) and 1.49 eV (**b**). **c-d** Comparison of a pulsed and CW excitation to show the broadening of the PL spectra when the material is excited to an EHP phase. **e-f** Nonlinear pump fluence PL dependence revealing that the lower the excitation energy, the greater the nonlinearity of the effect. All graphs in the top are for an excitation energy of 1.53 eV while the bottom graphs are for 1.49 eV. The axes of the (**e-f**) graphs are displayed in a logarithm scale.

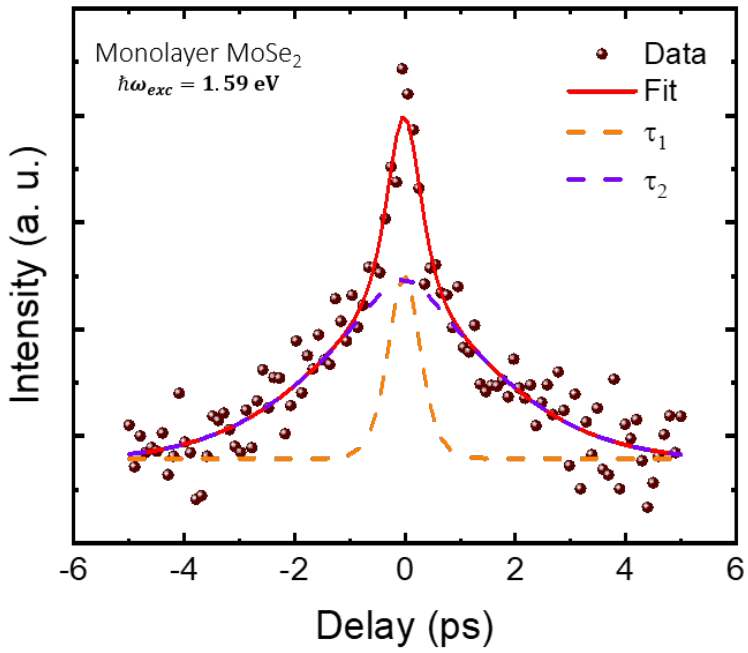

Figure S17: Two-pulse excitation correlation measurement in a monolayer $MoSe_2$. The scatter data show the intensity profile of the PL signal of a monolayer $MoSe_2$ sample with respect to the temporal delay between the incident laser pulses. We collected only the energies at 1.88 eV, above the band gap (1.62 eV) by using a combination of shortpass and bandpass filters. The temporal fit is shown in red, while the separated contributions of both time responses are displayed in the orange and purple dashed lines. It is observed a fast time scale of less than 100 fs and a slower one of ~ 4 ps.

Section S12. IRF Deconvolution

To extract the instrument response function (IRF) - that is mainly driven by the laser pulse width - we performed a second-harmonic generation (SHG) autocorrelation measurement in a $MoSe_2$ monolayer with the same optical setup of the two-pulse excitation correlation measurement. The SHG signal was directed to the spectrometer and its intensity as a function of the temporal pulse separation is shown in Figure S18. The autocorrelation data was fitted by a $sech^2(t/\tau)$ function (red dashed line) and yielded a laser pulse width value of $\tau = 375$ fs.

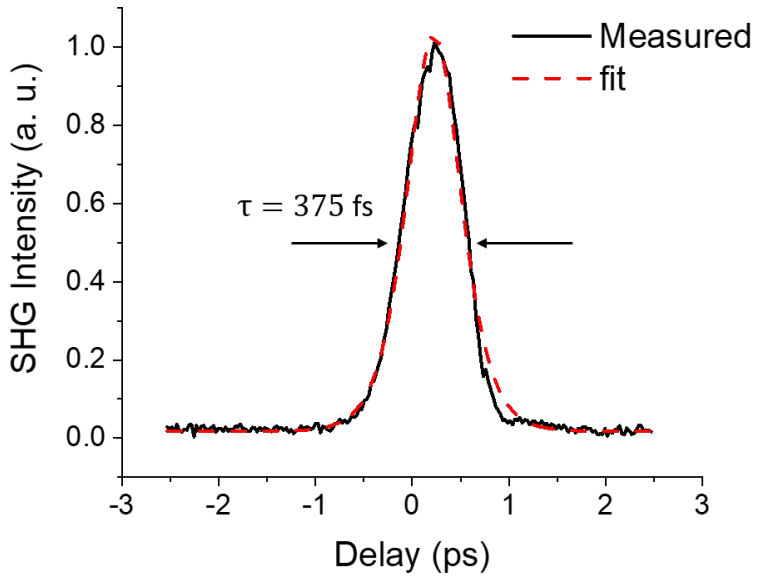

Figure S18: SHG autocorrelation measurement in a monolayer $MoSe_2$. The laser pulse width of 375 fs was extracted from the data fit (red dashed line).

In order to deconvolute the temporal response of the EHP PL signal from the laser pulse width response, we fitted our two-pulse excitation correlation data with the convolution of the intensity model function (Eq. 4 of the manuscript) with the $sech^2(t/\tau)$ function (IRF). This IRF deconvolution improved our temporal resolution to 100 fs.

SUPPORTING REFERENCES

[1] Zeng, H., Liu, G.-B., Dai, J., Yan, Y., Zhu, B., He, R., Xie, L., Xu, S., Chen, X., Yao, W., Cui, X. (2013). Optical signature of symmetry variations and spin-valley coupling in atomically thin tungsten dichalcogenides. Scientific Reports, 3(1), 1608. https://doi.org/10.1038/srep01608

[2] Tonndorf, P., Schmidt, R., Böttger, P., Zhang, X., Börner, J., Liebig, A., Albrecht, M., Kloc, C., Gordan, O., Zahn, D. R. T., Michaelis de Vasconcellos, S., Bratschitsch, R. (2013). Photoluminescence emission and Raman response of monolayer MoS_2, $MoSe_2$, and WSe_2. Optics Express, 21(4), 4908–4916. https://doi.org/10.1364/OE.21.004908

[3] Li, Y., Li, X., Yu, T., Yang, G., Chen, H., Zhang, C., Feng, Q., Ma, J., Liu, W., Xu, H., Liu, Y., Liu, X. (2018). Accurate identification of layer number for few-layer WS_2 and WSe_2 via spectroscopic study. Nanotechnology, 29(12), 124001. https://doi.org/10.1088/1361-6528/aaa923

[4] Jue, W., Jenny, A., Yusong, B., Alexander, S., Matthias, F., Frank, J., Xiaodong, X., Mackillo, K., James, H., X.-Y., Z. (2019). Optical generation of high carrier densities in 2D semiconductor heterobilayers. Science Advances, 5(9), eaax0145. https://doi.org/10.1126/sciadv.aax0145

[5] Li, Y., Chernikov, A., Zhang, X., Rigosi, A., Hill, H. M., van der Zande, A. M., Chenet, D. A., Shih, E.-M., Hone, J., Heinz, T. F. (2014). Measurement of the optical dielectric function of monolayer transition-metal dichalcogenides: MoS_2, $MoSe_2$, WS_2, and WSe_2. Physical Review B, 90(20), 205422. https://doi.org/10.1103/PhysRevB.90.205422

[6] Moody, G., Kavir Dass, C., Hao, K. et al. (2015). Intrinsic homogeneous linewidth

and broadening mechanisms of excitons in monolayer transition metal dichalcogenides. Nature Communications 6, 8315. https://doi.org/10.1038/ncomms9315